



Melt propagation and volcanism in mantle convection simulations, with applications for Martian volcanic and atmospheric evolution

C. O'Neill,^{1,4} A. Lenardic,¹ A. M. Jellinek,² and W. S. Kiefer³

Received 26 July 2006; revised 31 January 2007; accepted 30 March 2007; published 17 July 2007.

[1] Standard models for a warm, wet early Mars require a significant CO₂-H₂O atmosphere in the past. The source for these phases is assumed to be volcanic degassing. However, no consistent, dynamical models exist relating volcanic degassing to evolving mantle temperatures. Here we use a range of thermal, geophysical, geological, and petrological constraints from Mars to constrain mantle convection model simulations of Mars' post-Noachian stagnant lid evolution. We develop a methodology to self-consistently calculate melt extraction from the mantle source region. Using a dike-propagation algorithm, we can calculate the rate of volcanism and rate of volcanic degassing from these simulations and compare them with estimates for Mars. We find that Martian melt production rates are satisfied by a 200-km thick lithosphere (surface heat flow 25 ± 5 mW/m²) for an intermediate Martian solidus. Core-mantle temperatures cannot exceed $\sim 1850^\circ\text{C}$ from geodynamo constraints, and the enrichment of heat-producing elements into the crust is unlikely to exceed 25–50%. For hotter Martian mantle temperatures in the past, we find an evolution in rates of volcanism from >0.17 km³/yr for the early Hesperian to $\sim 1 \times 10^{-4}$ km³/yr at present, consistent with geological evidence. During this same interval, CO₂ flux would have declined from 8.8×10^7 to 6.7×10^6 kg/yr. If the early Hesperian supported a dense (>1 bar) atmosphere, this implies that the average loss rate of CO₂ from the atmosphere was 15 times greater than the maximum influx rate during this time.

Citation: O'Neill, C., A. Lenardic, A. M. Jellinek, and W. S. Kiefer (2007), Melt propagation and volcanism in mantle convection simulations, with applications for Martian volcanic and atmospheric evolution, *J. Geophys. Res.*, *112*, E07003, doi:10.1029/2006JE002799.

1. Introduction

[2] The existence of stable liquid water on the surface of early Mars requires significantly warmer surface temperatures generally associated with atmospheric pressures of several bars [Jakosky and Phillips, 2001]. Both these conditions minimally require increased volumes of volatiles, notably CO₂ and H₂O, in the Martian atmosphere in the past, supplemented by additional heating mechanisms [Forget and Pierrehumbert, 1997]. The volatile content of the Martian atmosphere is a function of the variation in replenishing and loss rates through time. Volatiles may be lost to space, locked in polar ice caps, react with surface minerals, or exist within the crust (for example, as groundwater) [Jakosky and Phillips, 2001]. The Martian atmosphere in the early Noachian (4.55–4.0 Ga) was probably efficiently

lost by hydrodynamic escape and large impacts [Jakosky and Phillips, 2001]. These processes do not induce isotope fractionations, and measurements of ¹⁵N/¹⁴N and ³⁸Ar/³⁶Ar in gas trapped in the meteorite ALH84001 show no fractionation, supporting the idea that impacts and hydrodynamic escape dominated atmospheric loss prior to 3.9 Ga [Marti and Mathew, 2000; Mathew and Marti, 2001]. Subsequent to this, loss through solar wind interactions (such as pick-up ion sputtering or hydrodynamic collisions) would become more important, resulting in the isotopic fractionation of the atmosphere observed presently [Jakosky and Phillips, 2001]. Most recent calculations based on the D/H atmospheric ratio indicate 60–90% of Martian water present in the Noachian has since been lost to space [Yung et al., 1988; Jakosky and Phillips, 2001].

[3] The primary source of most Martian volatiles is volcanic outgassing [e.g., Lunine et al., 2003], and thus volatile replenishment rates on Mars will be tied to the rate of volcanism through time. Evidence of recent volcanism on Mars comes from young (<2 Ma, Neukum et al. [2004]) lava flows of low crater densities, observed cinder cones near the North Pole [Garvin et al., 2000], the putative presence of atmospheric methane [Formisano et al., 2004; Lyons et al., 2005], and the young (160–180 Ma) ages of many Martian

¹Department of Earth Sciences, Rice University, Houston, Texas, USA.

²Department of Earth and Ocean Science, University of British Columbia, Vancouver, British Columbia, Canada.

³Lunar and Planetary Science Institute, Houston, Texas, USA.

⁴Now at GEMOC ARC National Key Centre, Macquarie University, New South Wales, Australia.

meteorites [Borg *et al.*, 2005]. That Mars is still volcanically active is fairly remarkable, given its small size and thermal state. Surface volcanism requires two criteria to meet: (1) mantle melting, a process that is probably very heterogenous and would generally occur at an active upwelling, so long as the lithosphere was thin enough to allow the warm upwelling material to exceed the solidus; and (2) extraction of mantle melts to the surface.

[4] Melt extraction occurs by a variety of multiscale processes in different tectonic settings [Hirschmann, 1995; Kelemen *et al.*, 1995; Rubin and MacDougall, 1988]. The critical limiting process in the eruption of mantle melts in most intraplate settings occurs in dike propagation. This includes feeder dikes propagating melt from the mantle source to shallow-level magma chambers, as is the case in Hawaii, or the direct emplacement of dikes propagating from the mantle source. Giant radiating dike swarms have been associated with many large igneous provinces on Earth, and dikes are probably the dominant migration mechanism for intraplate mafic melts [Ernst *et al.*, 2001]. Identification of giant radiating dike swarms on Venus and Mars [Ernst *et al.*, 2001] suggest dike propagation is an important volcanic process on one-plate planets. Indeed, most volcanism on these planets is probably perpetuated by feeder dikes from mantle sources. However, the relationship between mantle melting-dike propagation-volcanic degassing is not simple. The degree of melting in the Martian mantle depends critically on the lithospheric thickness, mantle temperatures, and distribution of heat production. The propagation of these melts as dikes depends on the local melt fraction, the overpressure due to the melt's buoyancy that is required to drive dike propagation, and the thickness and thermal state of the lithosphere [Rubin, 1995].

[5] The purpose of this paper is to introduce a self-consistent method for calculating melt extraction and rates of volcanism in mantle convection simulations using a model of dike propagation and interaction from the mantle source. The method will be used to constrain the post-Noachian volatile outgassing rates on Mars. The first two sections of this paper introduce the mantle/melting model for present-day Mars and a model for surface volcanism based on the efficiency of dike propagation from the mantle source. We extend our models back to the conditions of the late Noachian (~ 3.7 Ga) by increasing the concentration of heat-producing elements in the crust and mantle and derive a volatile degassing curve for Mars from 3.7 Ga to present. We combine our degassing rates with simple estimates of atmospheric loss rate through time to estimate the volatile content of the atmosphere/surface through time and constrain the time period during which liquid water may have been stable at the surface of Mars.

2. Model Description

2.1. Mantle Model

[6] The models presented here extend upon the one-dimensional [Weizmann *et al.*, 2001; Spohn, 1991] and earlier two-dimensional [Kiefer, 2003] convection models for Martian volcanism, in that we employ temperature-dependent viscosities to self-consistently determine the thickness of the lithosphere, internal temperatures, and the

Table 1. Physical Parameters Used^a

Symbol	Property	Value
ρ_m	Mantle density	3400 kg m ⁻³
g	Gravitation acceleration	3.72 m s ⁻²
α	Thermal expansivity	3×10^{-5} K ⁻¹
ΔT	Nonadiabatic temperature drop	1600 K (varies)
T_{CMB}	Temperature at the CMB	1800°C (varies)
d_m	Depth of convecting mantle	1698 km ^b
d_c	Crustal thickness	50 km
κ	Thermal diffusivity	10^{-6} m ² s ⁻¹
k	Thermal conductivity	3.5 W m ⁻¹ K ⁻¹
L	Latent heat of melting	6.4×10^5 J kg ⁻¹
C_p	Specific heat	1200 J K ⁻¹ kg ⁻¹
H	Mantle heat production	4.1×10^{-12} W kg ⁻¹ (varies)
E	Enrichment (crust)	0–1 (varies)
η_{mantle}	Mantle viscosity	10^{20} – 10^{25} Pas ⁻¹ (Arrhenius law)
Q	Effective activation energy	80–510 kJ/mol ^c
b	In viscosity exponent	r^c
$\Delta\rho$	Melt density contrast	400 kg m ⁻³
η_{melt}	Melt viscosity	10–100 Pas ⁻¹
dT_w/dz	Wall rock temperature gradient	From models, varies
M_{elas}	Elastic stiffness	20 GPa [= $G/(1 - \nu)$]
G	Modulus of rigidity	~ 15 Gpa
ν	Poisson's ratio	0.25
T_m	Melt temperature	Equal to solidus at same pressure
T_{vr}	Wall rock temperature	Ambient local solid temperature

^aAll values are the default unless explicitly stated otherwise. For references, see text, Kiefer [2003] and Rubin [1995].

^bAssume depth to the CMB for calculating Ra, rather than the thickness of the convecting mantle which is not defined a priori.

^cDepends on Arrhenius formulation; see section 3.1 for full discussion.

depth to which hot upwelling mantle ascends. The thermochemical convection calculations were performed using the particle-in-cell finite element code Ellipsis [Moresi *et al.*, 2003] in a two-dimensional Cartesian geometry. We use a 128-node grid in the vertical, with similar resolution laterally. The vertical grid is compressed by a factor of 1.5 in the top 10% of the modeling domain, where the greatest viscosity contrasts exists (10^5 over the whole system, most of which occurs in this region). The basal Rayleigh number, assuming the physical properties in Table 1 and using a temperature contrast of 1600 K, is $\sim 3 \times 10^7$. We also include internal heating in these models (discussed below). Other physical parameters used are listed in Table 1. We experiment with Arrhenius viscosity profiles, with varying viscosity contrasts. The realism of the viscosity structure of Mars strongly affects the depth of the lithosphere and the degree of melting.

[7] Fairly large uncertainties exist concerning the thermal structure of Mars. One the most important factors influencing Mars' thermal state is the concentration and partitioning of heat-producing elements (HPEs) in the Martian crust and mantle. Two models for Martian radioactivity exist: the models of Wanke and Dreibus [1994], based on Martian meteorites, and of Lodders and Fegley [1997], calculated from mixed chondritic compositions and fitted to oxygen isotope data. These data give present-day internal heating rates of 4.1 and 6.3×10^{-12} W kg⁻¹, respectively. Following Kiefer [2003], we adopt the former estimate as it better fits the K/U and K/Th ratios in Martian meteorites and gamma spectroscopy of the Martian surface [McLennan, 2001].

[8] The mean crustal thickness of Mars is assumed to be 50 km [Zuber *et al.*, 2000; Neumann *et al.*, 2004]. It has

been suggested that the formation of Southern Highlands on Mars would have depleted the mantle of over half of its inventory of HPEs [Spohn, 1991]. Tight constraints of the enrichment of the crust are, however, lacking. We consider a range of enrichment, from no relative enrichment of the crust to all the HPEs partitioned into the crust (i.e., no internal heat production in the mantle).

[9] Present-day Martian surface temperatures average about -53°C [Jakosky and Phillips, 2001]. On the basis of mantle-melting simulations, Kiefer [2003] constrained the temperatures at the base of the Martian mantle to be $\sim 1750\text{--}1850^{\circ}\text{C}$. Thermal-history modeling by Nimmo and Stevenson [2000] gives similar estimates. The Martian adiabatic gradient is assumed to be 0.18 K/km [Kiefer, 2003], resulting in an adiabatic contribution to the temperature gradient of 306°C at the base of the mantle. Thus a temperature at the core-mantle boundary (CMB) of 1800°C results in a nonadiabatic temperature difference of 1547 K to drive convection. The potential temperature of the Martian mantle is not set a priori; it arises as a consequence of the total nonadiabatic temperature gradient and internal heating rate (which vary back in the past and for different degrees of mantle depletion). For systems with temperature-dependent viscosities, the potential temperatures are primarily sensitive solely to these factors.

[10] Additional constraints on the thermal state of Mars arise from considerations of the surface and basal heat flow. McGovern et al. [2002, 2004] derived estimates for the elastic lithospheric thickness and heat flux using gravity and topography data. Estimates from recent (Amazonian, 0 to $\sim 2.9\text{ Ga}$) loading from the Tharsis volcanoes give heat flux estimates of $14\text{--}33\text{ mW/m}^2$. In comparison, Noachian heat flux estimates are upward of 45 mW/m^2 . These estimates provide useful constraints on thermal models of Mars. Additionally, the heat flux out of the Martian core must be less than 19 mW/m^2 or else the core would be convectively unstable, possibly allowing a geodynamo to operate [Nimmo and Stevenson, 2000]. While other factors may complicate whether or not a core dynamo may operate, it has been suggested that this low basal heat flow constraint is applicable to post-Noachian evolution of Mars, during which time the planet possessed no magnetic field [Nimmo and Stevenson, 2000].

2.2. Melting Model

[11] Bertka and Holloway [1994] determined the solidus for the dry undepleted Martian mantle composition by Wanke and Dreibus [1994], up to pressures of 3 GPa. They report low (1100°C) solidus temperatures at 0 GPa. Agee and Draper [2004] also constrained the solidus in the pressure range 5–9 GPa for the silicate portion of the Homestead L5 ordinary chondrite, believed to be of a similar composition to the Martian mantle. Musselwhite et al. [2006] calculated a depleted mantle solidus on the basis of the melting behavior of the Martian meteorite Yamato 980459, an olivine-rich shergottite. They report significantly higher (1440°C) solidus temperatures at 0 GPa, extending up to 1600°C at $\sim 1.7\text{ GPa}$. We explore a range of solidii encompassing these extremes.

[12] The presence of water in the mantle can significantly reduce the solidus temperature. However, Carr and Wanke [1992] and Norman [1999] constrain the water content of

the melt source region to be between 4 and 36 ppm, based on water content and degree of partial melt of Shergotty (cw. 100–450 ppm for midocean ridge basalt (MORB) on Earth; Sobolev and Chaussidon [1996]). Herd [2003] shows that the very low oxygen fugacity of many shergottites precludes the existence of free water in the source region. On the other hand, strong evidence now exists for the existence of free water on the surface of Mars in the past [Carr, 1996; Squyres et al., 2004; Catling, 2004]. We estimate the effect of a wet solidus on the degree of mantle melting by systematically lowering the solidus by several hundred degrees but suggest dry melting is more applicable for post-Noachian Mars.

[13] Direct estimates of the Martian mantle liquidus are limited. Agee and Draper [2004] estimate the difference between the solidus and liquidus temperature to be 200 K at 5 GPa. We adopt this difference to apply over the pressure range considered. While McKenzie and Bickle [1988] have shown that the melt fraction for peridotite melting on Earth has a third-order polynomial relationship with the super-solidus temperature, to a first degree a good approximation is obtained by considering a linear relationship between melt fraction and supersolidus temperature [Jaques and Green, 1980]. The supersolidus temperature T_{ss} is defined by:

$$T_{ss} = \frac{T - T(P)_s}{T(P)_l - T(P)_s} \quad (1)$$

where T is the temperature, P is the pressure, and the subscripts s and l refer to the solidus and liquidus temperatures at P . The melt fraction F is equal to T_{ss} . Latent heat of melting can have an important effect locally in modulating further melt production, and we model this effect by including a latent heat term in the energy equation [O'Neill et al., 2005].

[14] We do not consider the ongoing depletion of the mantle due to melt extraction in this study; this is history dependent, irreversible, and strongly influenced by the initial thermal configuration of a system. Instead, we assume when the melt fraction reaches a critical density (2% for peridotite melting; Turcotte and Schubert [1982]), melt percolates into a network of veins and channels and becomes concentrated on a scale below the resolution of our model (i.e., subparticle scale). To convert two-dimensional melt “areas” into melt volumes for comparison with Martian constraints, we make the assumption that the discrete melt regions are cylindrically symmetric (which is approximately valid if the active upwellings are plumes), then integrate these discrete melt regions around a center axis to obtain a volume. This local volume of this melt depends both on a particle's local volume and melt fraction. As we will show, these local melt volumes exceed the necessary criteria for dike propagation, and so extraction from the source region occurs primarily by this mechanism [Rubin, 1998].

2.3. Model for Melt Propagation and Surface Volcanism: Constraints and Limitations

[15] The extraction of melt from the mantle in intraplate settings is not fully understood, and any model of it inevitably simplifies the physical reality. In the first stage of melting, melt migrates by porous flow through an interconnected

network, when melt fractions reach a critical percentage ($\sim 2\%$). These melts generally coalesce to form a dike in order to propagate through the lithosphere. The intermediate steps, from the coalescence of percolating melt to form a network of veins and channels to finally reaching the critical volume for dike formation, is not well understood in intraplate settings.

[16] A number of constraints exist of the physical processes of melt extraction from the source region. First, the spacing of volcanoes in island arc settings may give an indication on the extent of the local source region [Hieronymus and Bercovici, 2001]. However, the volcanic spacing seems largely controlled by lithospheric flexure due to the loading of the volcanoes [ten Brink, 1991; Hieronymus and Bercovici, 1999]. U-series systematics seem to suggest an extremely short period of time between extraction from the mantle and eruption (less than ~ 1000 years; Bourdon *et al.* [2005], Turner *et al.* [2001]). This is extremely fast; in fact, this time is less than the characteristic timestep of a convection simulation and thus cannot be resolved dynamically in these models. One implication of this is that we inherently assume intermittent pulses with longer magma supply lags in between; and the volume flux during such pulses will exceed the long-term average. Another implication of this short extraction time is that there is limited time for magma storage prior to eruption; that is, the residence time in magma chambers during magma ascent is either short or does not occur.

[17] This leads us to another constraint on magma transport: magma buoyancy. The melting of mantle peridotite, with a density of ~ 3300 kg/m³, generally produces melts of basaltic composition ($\rho \sim 2900$ kg/m³). The density difference between the melt and residue creates a critical overpressure driving the melt toward the surface. For large dike lengths typical for the eruption of mantle melts (> 1 km), the pressure due to the buoyancy of the melt dominates other sources of pressure, such as magma chamber overpressure or ambient tectonic stresses [Rubin, 1995]. The critical overpressure can be calculated assuming Archimede's principle, namely, that the pressure is equal to the mass of the fluid displaced, $\Delta\rho gV$, where V is the volume of melt. This overpressure may change when the dike passes a density transition in the lithospheric column, such as at the crust-mantle boundary. Here the magma may no longer be intrinsically buoyant, and it may stall. Lister [1990] showed that the magma may overshoot this transition by some amount. Additionally, the addition of volatiles may provide an excess magma buoyancy enabling upward propagation to continue. In the case of Mars, if we assume the majority of the crust to be of a primarily basaltic composition, then a magma of similar composition will possess enough intrinsic density to rise to the surface. Exsolving volatiles may reduce the magma density even further.

[18] Thus we have the following limitations on our model: (1) we assume that melt is channeled and coalesces in timescales less than the characteristic timescale of the simulation. Thus at each new timestep we have a "finite volume" of melt which propagates toward the surface. (2) We have neglected magma storage during ascent and assume either dikes freeze out during their ascent or erupt. (3) Because of the lateral and vertical heterogeneity of the Martian crust and the poorly constrained density of Martian melts, we have neglected the effect of density changes in the host rock during

magma ascent. This is a fairly severe assumption and one that should be addressed in further work. In the severe case of grossly overestimating melt buoyancy and overestimating crustal densities, this approach may overestimate volcanic rates by up to a factor of 3. Other approaches, such as calculating the critical overpressure required to pressurize a preexisting magma-filled fracture to enable it to propagate from the level of neutral buoyancy to the surface [Jellinek and DePaolo, 2003], may be useful in resolving the emplacement mechanism. However, our goal here is primarily to introduce a technique for calculating melt extraction from the mantle. Thus the final emplacement of melt will result in the emplacement of new crust regardless, though our estimates of volcanism and volatile escape may be too high.

2.4. Propagation of a Single Dike

[19] The first constraint to be satisfied in order for a dike to become self-propagating is that the elastic stresses generated by the dike must exceed the fracture toughness of the rock, K_c . This is formalized in the definition of the crack-tip intensity factor K , where

$$K = 1.12\Delta P_c(l)^{1/2} \quad (2)$$

[20] Here ΔP_c is the critical overpressure, and l is the dike length. That $K > K_c$ is a necessary condition for dike propagation. This condition is shown in Figure 1a for increasing magma chamber volume (and, subsequently, increasing magma buoyancy and ΔP_c). In this case, the magma source is assumed to be at 100 km depth, and the dike length l is fixed at this value. The critical K_c , of around $1-10$ MPam^{-1/2}, is reached for rather minor melt volumes (~ 10 m³). In fact, for a nominal $\Delta P_c \sim 1$ MPa, this elastic fracture criterion is met if dike lengths exceed few meters and thus should be generally met in most mantle-melting events. An important caveat to this is the criterion may be more stringent if (1) we consider the increase in fracture toughness of the rock with depth [Sato and Hashida, 2006], and (2) we consider the decrease in melt buoyancy with pressure [Stolper *et al.*, 1981]. Both factors will sizably increase the magma volume required for a hydrofracture event by up to a factor of 3–4.

[21] In any case, the fracture criterion is in itself is an insufficient condition to ensure that a dike will propagate from its mantle source to the surface. As a dike intrudes into cooler host rock, it will itself cool, become more viscous, and eventually freeze. Rubin [1995] argues that a dike will only propagate if the flow rate into the dike is sufficient that the dike widens faster than it narrows as a result of freezing. This condition is encapsulated in the dimensionless parameter β :

$$\beta = 2 \left(\frac{3\kappa\eta_m}{\pi\Delta P_c} \right)^{1/2} \frac{c|dT_{wr}/dz|}{L} \left(\frac{\Delta P_c}{M_{elas}} \right)^{-2} \quad (3)$$

[22] Here κ is the thermal diffusivity, c is the specific heat, η_m is the magma viscosity, L is the latent heat of melting, dT_{wr}/dz is the temperature gradient in the wall rock along the dike path, and M_{elas} is the elastic stiffness. If the calculated value is less than the critical value of 0.15, the dike will survive transport. We calculate β for typical conditions

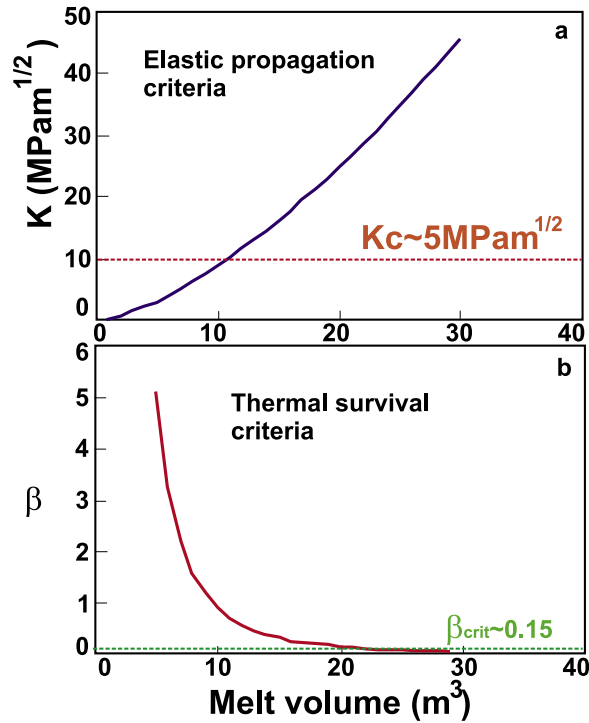


Figure 1. (a) Crack tip intensity factor K versus melt volume (equation 2). The critical fracture toughness Kc for most rocks is between 1 and 10 MPam^{1/2}. This criterion is met in most mantle melting events for very small volumes (<10 m³) of melt. (b) Thermal survival parameter β versus melt volume (equation 3). We adopt representative physical values for a mafic dike in a mantle source outlined by Rubin [1995]. The critical β for the thermal survival of a propagating dike is 0.15, a condition that is met for fairly small (>21 m³) melt volumes. This small volume may be revised if we consider (1) decreases in melt buoyancy with depth [Stolper *et al.*, 1981] and (2) increase in the critical fracture toughness with depth [Sato and Hashida, 2006].

of a basaltic dike in a mantle source in Figure 1b (see Rubin [1995] for details). As the melt volume increases, so does ΔP_c , and the critical value of $\beta \sim 0.15$ is met for melt volumes of around 21 m³. This is a very small melt volume and suggests that mafic dikes will be fairly ubiquitous wherever mantle-melts pond in even minor volumes.

[23] While β describes whether a dike will propagate or not, it does not constrain how far. The timescales for dike formation and propagation are significantly less than the timescales for melt supply by adiabatically decompressing mantle flow. Additionally, for large dikes, it is unrealistic to assume constant source pressure. Thus for our problem, we consider the problem of finite volume source, which is discussed by Lister [1994]. This formulation neglects elasticity and assumes that the fundamental control on dike propagation is the freezing of magma from the dike walls inward. Assuming the magma temperature is at the solidus ($T_m = T_s$), the maximum height of ascent is:

$$h_f = 0.48\lambda^{2/5} \left(\frac{3}{4}A\right)^{4/5} \left(\frac{\Delta\rho g}{\eta_m \kappa}\right)^{1/5} \quad (4)$$

[24] Here A is the cross-sectional area of the dike, $\Delta\rho$ is the density contrast between the melt and host rock, g is gravity, η_m is the magma viscosity, and κ is the thermal diffusivity. The parameter λ is defined by a transcendental equation, arising from the Stefan problem for the solidification of a dike [Turcotte and Schubert, 1982]:

$$\frac{e^{-\lambda^2}}{\lambda(1 + \operatorname{erf}\lambda)} = \frac{L\sqrt{\pi}}{c(T_m - T_{wr}(z))} \quad (5)$$

[25] Here erf refers to the error function, T_m is the magma temperature, and $T_{wr}(z)$ is the temperature of the wall rock at depth z . This function can be solved numerically or can, for small λ , be linearized to:

$$\lambda = \frac{c(T_m - T_{wr}(z))}{\pi^{1/2}L} \quad (6)$$

[26] If the source depth is shallower than h_f , then the fraction of basalt erupted can be estimated from the ratio of h_f to the source depth. This is shown in Figure 2. For small magma chambers (100 m × 100 m × 100 m, ~0.001 km³), limited melt volumes constrain A in equation (4). Thus while the dike will certainly propagate, it will only be able to propagate ~24 km, far short of erupting on the surface in this example. For greater melt volumes, h_f greatly exceeds the depth to the melt source, and the volume erupted in these circumstances is $(h_f - d_{\text{source}})/h_f$ times the generated melt volume.

2.5. Size of the Source Region

[27] As evidenced in the above examples, the size of the source region of mantle dikes plays a controlling role in whether a dike will erupt at the surface or not and what fraction of available melt will be erupted. However, what is the scale of this source region? As we have shown, mafic dikes will propagate at extremely low melt volumes; and at one extreme, we have the case where any small ponding of melt will result in the formation of a small dike which travels a minimal distance before freezing. Under these conditions, it is difficult to generate sufficient melt volumes to erupt through a thick, intact lithosphere. On the other hand, mantle melting in actively upwelling zones can occur on scales on several hundred kilometers. Assuming melt percolates by porous/reactive flow in the actively melting regions, there is the potential to concentrate massive melt volumes, which would generate giant dikes with eruption efficiencies approaching 100%.

2.5.1. Coalescence of Dikes

[28] The problem is rate-dependent, in that whenever melt generation rates exceed the rate of cooling of small dikes, minor dikes will become overwhelmed and coalesce to form larger intrusive structures. Takada [1989] presented a model of interacting propagating cracks. Additionally, Ito and Martel [2002] showed that as rising dikes affect the local stress field, they will mechanically interact and affect each other's ascent path. The strength of the interaction and its style (whether repulsive or attractive) depends on the horizontal and vertical displacements between the two dikes. The behavior is summarized in Figure 3. No interaction occurs if the dikes are too widely spaced. If the

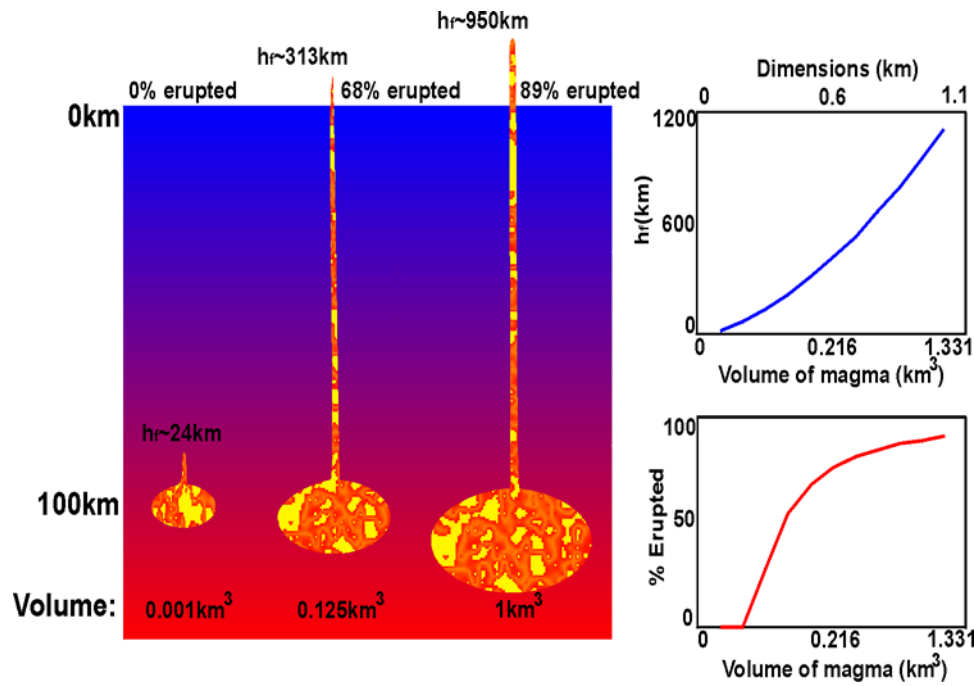


Figure 2. Maximum height of ascent h_f versus magma volume [equation (4)]. For small magma volumes, the distance the dike will propagate before freezing out is less than its depth (100 km in this example), and it will not erupt. For greater magma volumes, the height of ascent exceeds the depth of the magma source, and it will erupt. The percentage erupted can be estimated from the height of ascent maximum height of ascent and the depth of the magma source. (b) Volume of magma (log scale, bottom) or dimensions of magma chamber (top) versus the maximum height of ascent, calculated from equation (5). (c) Percentage of magma erupted versus volume of magma.

spacing between dikes is less than the dike length scale, their stress fields will interact. In this case, if two dikes are at equal depths, the interaction of their stress fields tends to cause repulsion. If the two dikes are at different depths, then

they will coalesce, and the strength of this coalescence depends on their proximity.

2.5.2. Parameterised Model and Benchmark

[29] The mantle convection code we use, Ellipsis, is based on a fixed Eulerian mesh but contains particles which act as

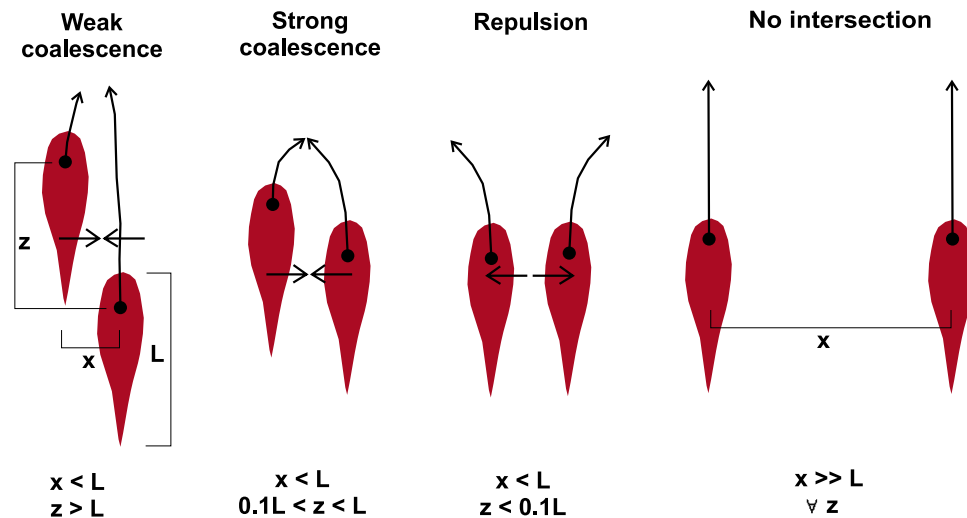


Figure 3. Summary of the interaction of ascending dikes, from the study of *Ito and Martel* [2002]. Propagating dikes affect their local stress field and will coalesce or repulse depending on their relative positions. Dikes will coalesce if their horizontal spacing x is less than the dike length L , providing they are offset vertically by at least $0.1 L$. If they are not offset by $0.1 L$, the dikes will repulse each other. Additionally, if the horizontal separation between the dikes is much greater than the dike length, they will not interact.

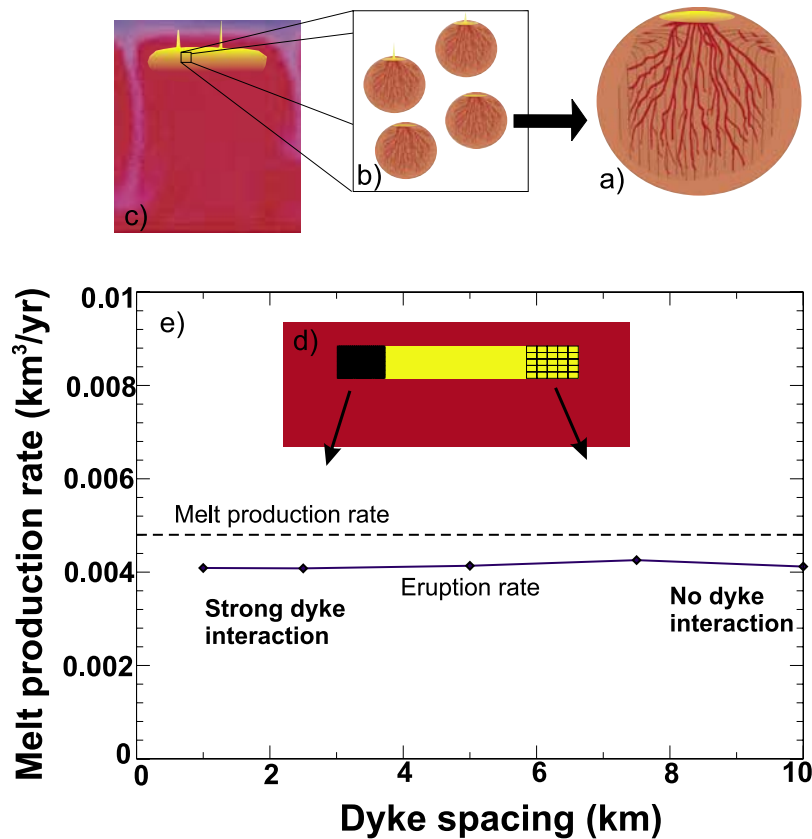


Figure 4. Model for melt migration and benchmark. (a) At the finest scale (individual particles), melt is assumed to rapidly coalesce by channeled flow into a finite volume, the size of which is determined by the particle's local volume and melt fraction. (b) This finite volume may or may not be sufficient for dike propagation [equations (2) and (3)]; if so, (c) dikes will propagate a finite distance [equation (4)] and may coalesce (Figure 3) and/or erupt at the surface. (d) Resolution test of our dike propagation/interaction algorithm; Artificial mantle, melting zone configuration. We predefine a melt region between 40 and 120 km in depth and 200 km wide, with an instantaneous melt production rate of $0.0048 \text{ km}^3/\text{yr}$ (light). This melting zone is sampled by grids of various resolutions, representing initial dike spacings of 1–10 km. These sample points represent a local volume defined by the resolution of the grid. (e) Eruption rate versus dike (or grid) spacing. At a large grid/(dike) spacing of 10 km, the few large, widely spaced dikes do not interact and carry most the melt to the surface. At finer dike spacings ($\sim 1 \text{ km}$), the smaller dikes are unable to propagate to the surface but interact strongly because of their close spacing. They eventually form a few, large dikes which transport most of the melt to the surface. The eruption efficiency ($\sim 83\%$) is only weakly affected by the resolution.

integration points, are advected with the flow, and carry important history-dependent information about the material such as depletion. The particles represent the finest subdivision of the problem and are typically of the scale of a few kilometers. Clearly this is far larger than the length scale of melt features such as veins and dikes. Given this constraint and the resolution of the timestep compared to melt extraction time, we make the assumption that melt is focused and coalesces into finite volumes within individual particles at each time step. That is, given a certain average melt fraction of a particle and knowing its local volume, we can estimate the volume of melt produced. We assume this melt is rapidly extracted by channelized flow to form a coherent magma body on a timescale less than the simulation's timescale. These magma bodies, existing at the position of the particle, then form dikes. Whether such dikes can propagate or not

depends on the satisfaction of equation (3). The height to which they propagate is determined by equation (5). Their behavior with respect to surrounding dikes is governed by the criteria of *Ito and Martel* [2002]. A potential issue with using the local volume of particles to determine melt volumes is: Does the erupted melt volume depend on the local volume of the particles? That is, if we have a low-resolution simulation, with few particles of large volumes, and a high-resolution simulation, with many particles of smaller local volumes, is the eruption efficiency affected?

[30] We have included this empirical description of dike interaction in our models to consistently self-determine the scale of the melt source region. We show the results of a resolution test on an algorithm describing this behavior in Figure 4. Here we have predefined a melt region between

40 and 120 km in depth and 200 km wide, with an instantaneous melt production rate of $0.0048 \text{ km}^3/\text{yr}$. This melting zone is sampled by grids of various resolutions, representing initial dike spacings of 1–10 km. These sample points represent a local volume defined by the resolution of the grid. At a large grid (/dike) spacing of 10 km representing a large local volume of melt, melt is efficiently carried to the surface, and the widely spaced dikes do not intersect. At finer dike spacings (~ 1 km), the ability of individual dikes to propagate to the surface is diminished, and the closely spaced dikes show a much greater proclivity to interact. This results in the agglomeration of a few, large dikes which transport most of the melt to the surface. The eruption efficiency ($\sim 83\%$) is only weakly affected by the resolution.

3. Results

3.1. Viscosity Structures

[31] One of the most important controls on Martian melt production is the lithospheric thickness. *Kiefer* [2003] showed how small changes in lithospheric thickness can completely shut off melting in the Martian mantle. The mechanical lithosphere, i.e., that part that does not participate in convection, is essentially equivalent to the thermal boundary layer (TBL) and is essentially defined by the temperature gradient between the mantle interior and the surface and the vigor of convection (described by the Rayleigh number). The Rayleigh number itself is a function of the average internal viscosity, which again is strongly dependent on the internal temperatures. Thus there are important feedbacks between the interior mantle temperatures and the depth to which plumes can rise (lid thickness, i.e., the thickness of the nonconvecting portion of the surface boundary layer). Both these factors strongly affect mantle melt production and need to be determined self-consistently. This is an important advance over previous studies and one which will strongly affect our results. Previous work with stagnant lid convection [e.g., *Moresi and Solomatov*, 1995] have shown that the internal temperatures of such systems are much greater than equivalent isoviscous or mobile-lid systems.

[32] We explore the effect of different viscosity structures in Figure 5. An important distinction between isoviscous cases and temperature-dependent viscosity examples is that with a temperature-dependent viscosity, cold material tends to convect very sluggishly. This inefficient advection of heat causes the system to heat up and subsequently convect faster, and the tendency is that temperature-dependent viscosities result in higher internal temperatures and more melting than equivalent isoviscous cases. This is, however, strongly provisional on lid thickness.

[33] In our temperature-dependent viscosity examples, this lid thickness is self-consistently determined by the rheology and temperature gradient. Laboratory experiments have shown that the mantle follows an Arrhenius temperature dependence [*Karato and Wu*, 1993]. Because our models are solved for nondimensional temperatures between 0 and 1, we adopt the following form for the Arrhenius viscosity:

$$\eta = A e^{(Q_1/(T+b))}. \quad (7)$$

[34] The constant b we use to avoid singularities when $T = 0$. A is the viscosity scaling factor, and Q_1 is related to an activation enthalpy, compared to the standard Arrhenius form (such as used by *Karato and Wu* [1993]).

[35] The lack of surface deformation for the last 3 Gyr suggests that the predominant mode of convection on Mars for most of its history is stagnant lid convection. We adopt a viscosity contrast (10^5) sufficient to place us firmly within the stagnant lid regime. Larger viscosity variations are increasingly difficult to solve and primarily affect the uppermost portions of the immobile lid and not the bulk internal viscosities (Figure 5, cw. *King and Masters* [1992]). Furthermore, the uppermost portions of the lid where these large viscosity gradients occur would, if stressed, fail by brittle-fracture or plastic mechanisms rather than viscous flow.

[36] We have tested the sensitivity of the viscosity gradient across the rheological boundary, which drives the internal flow, to varying viscosity contrasts. The effect of increasing viscosity contrast on lid thickness is less than variations within a lid thickness for a given viscosity contrast. The rheological boundary layer thickness is strongly sensitive to mantle thermal structure, and variations within a given model are greater than variations between different viscosity contrasts. The viscosity contrast across the rheological boundary layer is less than an order of magnitude in all cases.

[37] Support for extremely large viscosity contrasts with temperature within the mantle come from the work of *Karato and Wu* [1993], who calculated plausible activation energies (200–400 kJ/mol) which suggest viscosity contrasts of the order of $>10^{40}$. Such contrasts are not reliably treated by our code's solver, but we have made a comparison between a viscosity contrast of 10^5 and 10^{40} but with a viscosity cut-off for the latter imposed at 10^6 (nb we derive Q_1 and b to simultaneously satisfy a 10^{40} viscosity contrast in a nondimensional system with a temperature contrast of 0–1). The results of this are shown in Figure 5c. The average lithospheric thickness is slightly greater for the 10^{40} case, but the fundamental observation remains that the variability in the viscosity gradient over the rheological boundary layer, even within a model at a certain timestep, is greater than the systematic variation with increasing viscosity contrast. The viscosity drop over the rheological boundary layer is similar in both cases (i.e., less than an order of magnitude, factor of ~ 8). The interior velocities are comparable in both cases.

[38] Another form of the Arrhenius viscosity more commonly used recently adopts an exponent of (Q_2/RT) , where Q_2 is the activation energy (strictly, the activation enthalpy, but we are ignoring pressure effects), and R is the gas constant [*Reese et al.*, 1999]. The gradients between this formulation and equation (7) are slightly different, but a comparison between the two can be made at a given temperature. For a surface temperature of ~ 220 K and a viscosity contrast of 10^5 , the exponent is ~ 44 . Equating this to (Q_2/RT) for the same temperature and $R = 8.314$ gives us an activation energy of ~ 81 kJ/mol. This is low, but new studies of seamount loading have suggested activation energies of 120 kJ/mol with asthenospheric viscosities of ≤ 20 Pa s [*Watts and Zhong*, 2000]. For interior temperatures of ~ 1800 K, the exponent is ~ 34 , giving an

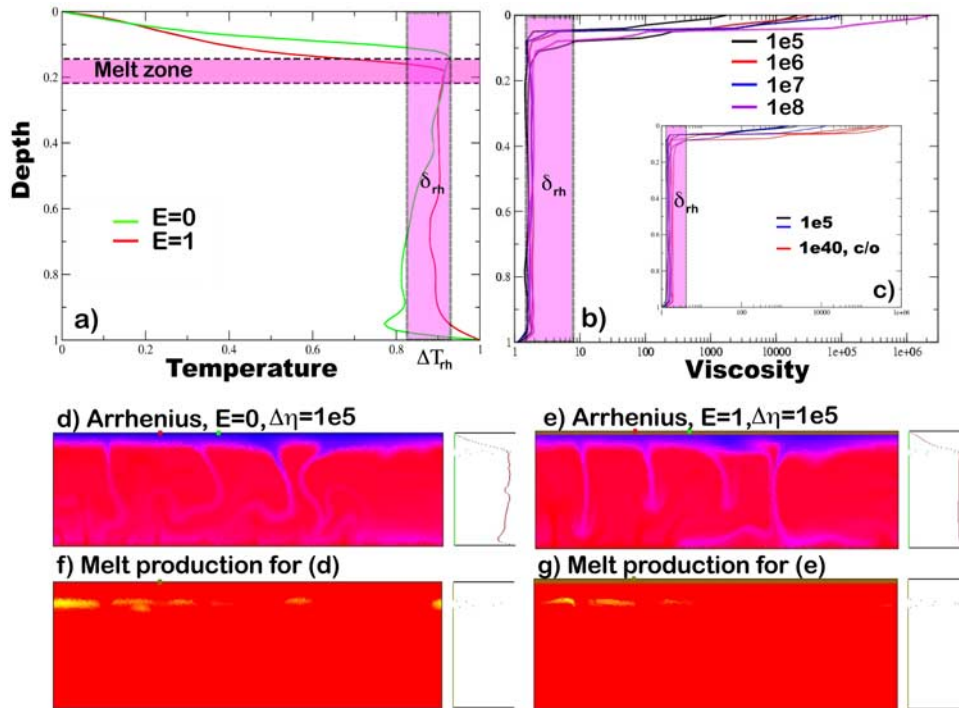


Figure 5. Effect of viscosity structure on mantle configuration and melt production. (a) Nondimensional temperature versus depth, horizontally averaged for the whole system. The sublithospheric melt-zone for the Martian solidus of *Bertka and Holloway* [1994] is shown. δ_{rh} denotes the rheological boundary layer, and ΔT_{rh} shows the temperature contrast across it. The enrichment value in the legend is here denoted by “E”. (b) Viscosity profiles for Arrhenius viscosity relationships with different total viscosity contrasts (10^5 – 10^8). The profiles are constructed by interpolation from particle tracers and so do not reach the maximum nodal viscosities near the surface. Examples are shown for 10^5 – 10^8 , from different parts of the lid (i.e., not averaged as in Figure 5a), showing the variation within a given simulation is as large as the variation in lid thickness for increasing viscosities within the range explored. δ_{rh} denotes viscosity contrast across the rheological boundary layer. (c) Comparison of three viscosity profiles from two different timesteps for a contrast of 10^5 and three profiles for a viscosity contrast of 10^{40} with a maximum viscosity cutoff imposed at 10^6 . (d–g) Examples of stagnant lid convection with Arrhenius viscosity which varies over 5 orders of magnitude, with a basal Rayleigh number of 3×10^7 . All models have periodic boundary conditions, and normalized temperature/melt production profiles are shown to the right. The examples are for no crustal enrichment of heat production or the extreme case where all heat production is concentrated in the crust, for the Martian solidus of *Bertka and Holloway* [1994] (Figures 5d and 5e are temperature fields, Figures 5f and 5g show melt production).

activation energy of ~ 510 kJ/mol. The two are different, as the gradients between the two formulations are not directly comparable, but encompass an acceptable range of activation energies. Variations between the two formulations predominantly occur in the stagnant upper boundary layer and do not significantly alter the style of convection. The important thing for this study is we have (1) plausible viscosity gradients and total viscosity contrasts over the rheological boundary layer; (2) plausible, if variable, rheological boundary layer thicknesses; (3) plausible velocities within the rheological boundary layer and the convecting interior; and (4) acceptable temperature contrasts across the rheological boundary layer.

[39] Furthermore, the lithospheric thickness in this example is around 200 km, similar to estimates for Mars based on elastic lithospheric thicknesses. The average surface heat flux in this example (25 ± 5 mW/m²) is also very similar to estimates of the recent heat flow of the Tharsis rise [*McGovern*

et al., 2002, 2004]. Given this consistency and that the effect of unknown compositional variations or volatile variations will have far greater effects on the effective viscosity, and for computational speed and accuracy, we use a viscosity contrast of 10^5 from here on.

[40] Interestingly, the warmer interior temperatures in our temperature-dependent viscosity examples result in mantle melting for all values of crustal enrichment, from primitive mantle to all HPEs concentrated in the crust. This is in contrast to the simulations of *Kiefer* [2003], who found mantle melting ceased at a critical depletion value. The difference between the two results is primarily due to the higher internal temperatures in our simulations but suggests that, for the solidus of *Bertka and Holloway* [1994], mantle melt production cannot “by itself” constrain the degree of crustal enrichment on Mars. We discuss this further in the following sections.

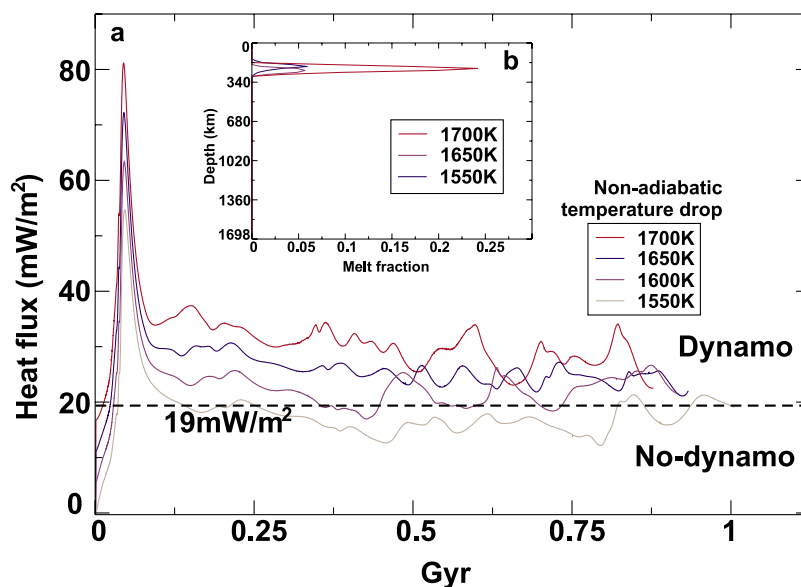


Figure 6. (a) Core-mantle heat flux versus time for a number of simulations with different nonadiabatic temperature drops across the convecting mantle. Models similar to Figure 5 and described in text. All model parameters (including heat production) are held constant, and the model is allowed to run to steady state. The large initial peak in heat flux is a transient feature resulting from our nonsteady state starting conditions. If the nonadiabatic temperature drop exceeds 1600 K (equivalent to temperature at the CMB of 1853°C), then core heat flux should be enough to power a geodynamo. The lack of a global magnetic field on Mars suggests that temperatures at the CMB do not exceed $\sim 1850^\circ\text{C}$. (b) Melt fraction profiles for the three listed nonadiabatic temperature drops. The extremely high melt fractions, a temperature drop of 1700 K (CMB temperature of 1953°C), provides an additional argument against a hot Martian CMB, though the extreme depletion in some shergottites [Musselwhite *et al.*, 2006] suggests this could be locally important during Tharsis’s history.

3.2. CMB Temperatures

[41] A dominant factor in the internal temperatures of the Martian mantle is the nonadiabatic temperature difference across the mantle available to drive convection. We have assumed a nominal temperature drop of 1547°C , equivalent to a basal temperature of 1800°C . The effect of changing this is shown in Figure 6.

[42] The high internal temperatures strongly modulate the temperatures in upwelling plumes, and the melt production rate is only weakly dependent on the temperatures at the base of the mantle. However, the temperature drop across the lower thermal boundary layer, and thus the average basal heat flux, is strongly a function of CMB temperatures. Increasing the CMB temperatures to 1853°C (equivalent to a 1600°C nonadiabatic temperature drop) results in basal heat fluxes in excess of 19 mW/m^2 , which would cause the core to convect and potentially power a dynamo [Nimmo and Stevenson, 2000]. If we take the lack of a present Martian magnetic field as a constraint on the CMB heat flux, then the temperatures at the CMB presently should not exceed $\sim 1850^\circ\text{C}$. Of course, there are large uncertainties in the critical heat flux value of 19 mW/m^2 , of the order of a factor of 2 [Nimmo and Stevenson, 2000], and additional geometric uncertainties are introduced by our regional-scale Cartesian grid (as opposed to a global spherical geometry). In all, the critical CMB heat flux temperature has an uncertainty of probably at least a factor of 2–3, although it is increasingly difficult to reconcile models with the evidence for more extreme values.

3.3. Effect of Solidus/Liquidus Variations

[43] Mantle melt production rates are strongly sensitive to the assumed solidus. Figure 7 shows the effect varying the solidus temperature (at zero pressure) has on the extent of mantle melt production. The solidus of Bertka and Holloway [1994] is based on average mantle compositions before crustal extraction and is probably an underestimate of the average Martian mantle solidus for the Hesperian and Amazonian. It also gives an unrealistically high melt production rate for our stagnant lid models. This again contrasts with Kiefer [2003] and is a result of the higher mantle temperatures in simulations with temperature-dependent viscosities. At the other extreme, the solidus for Martian meteorite Yamato determined by Musselwhite *et al.* [2006], at 1440°C at zero pressure, is extremely high, reflecting its very high olivine abundance. However, this composition is probably not representative of the bulk of the Martian mantle. It results in no melt production for our “Amazonian” models. Understanding the high temperature origin of the Yamato 980459 melting event and its possible relationship to deep thermal or chemical heterogeneities in the Martian mantle remains an important challenge that we leave to future work.

[44] The volcanic resurfacing rate on Mars for the midlate Amazonian has been estimated at $10^{-2}\text{ km}^2/\text{yr}$ [Tanaka *et al.*, 1992; Hartmann and Neukum, 2001]. On the basis of the assumed thickness of lava flows (3–10 m), this equates to a volumetric eruption rate of $0.3\text{--}1 \times 10^{-4}\text{ km}^3/\text{yr}$. From this, Kiefer [2003] estimates a recent melt production rate of $0.15\text{--}2 \times 10^{-3}\text{ km}^3/\text{yr}$ assuming an eruption efficiency of

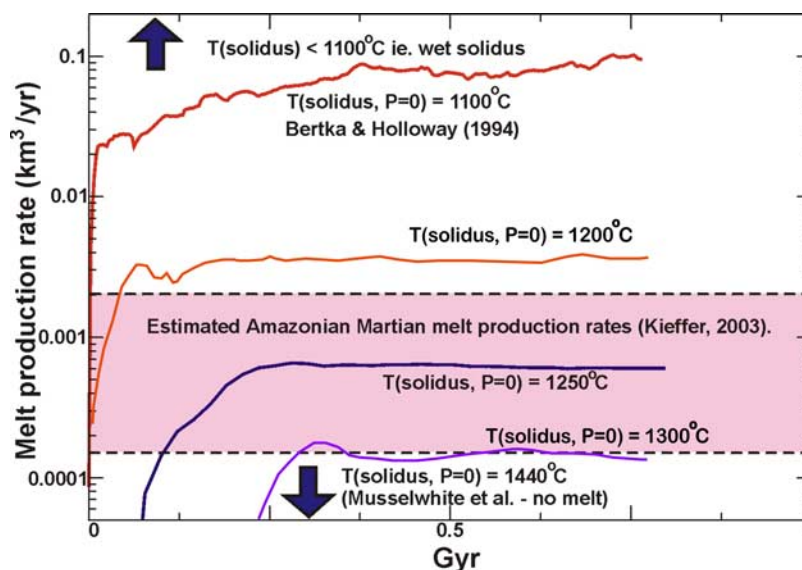


Figure 7. Mantle melt production rate versus time for models similar to Figure 5, with material properties listed in Table 1. For a surface solidus temperature by *Bertka and Holloway* [1994] of 1100°C or less, the melt production rates exceed the estimated Amazonian Martian melt production estimates of *Kieffer* [2003] (shaded region). For extremely high surface solidus temperatures, such as that of *Musselwhite et al.* [2006], no mantle melting occurs. For this model, we find an acceptable melt production rate for a surface solidus temperature of 1250°C, intermediate between the undepleted solidus of *Bertka and Holloway* [1994] and the extremely depleted shergottite solidus of *Musselwhite et al.* [2006].

5–20%. The current volcanism rates on Mars can be matched for our “Amazonian” mantle model by a solidus intermediate between the undifferentiated example by *Bertka and Holloway* [1994] and the extremely depleted solidus of *Musselwhite et al.* [2006]. Because of limited Martian samples, no melting experiments exist on a sample intermediate between *Wanke and Dreibus’s* [1994] undifferentiated Martian mantle case and the extremely depleted Yamato 980459 shergottite. However, a solidus representative of the average Martian mantle is likely to fall between these extremes, and in the absence of any specific constraints, we assume its starting temperature to be 1200–1300°C at zero pressure.

3.4. Mantle Depletion: Crustal Enrichment

[45] Obviously, there will be a play-off between solidus temperature and the level of crustal enrichment; higher solidus temperatures will require lower levels of crustal enrichment to maintain a permissible melt production rate. With that in mind, Figure 8 shows the relationship between the eruption rate and level of crustal enrichment for 1250°C surface solidus temperature. For low levels of crustal enrichment, high heat production in the mantle results in significant ($>5e-4$ km³/yr) eruption rates, in excess of estimated volcanic resurfacing rates for Mars [*Tanaka et al.*, 1992; *Hartmann and Neukum*, 2001]. Increasing the crustal enrichment systematically decreases the mantle temperatures and subsequently the mantle melt production rates. For enrichment values in excess of 50%, no melting occurs. For a 1250°C solidus temperature, allowable levels of crustal enrichment are between ~ 25 and 42%. Note that the quantity plotted in both Figures 8 and 9 is the surface eruption rate rather than the total melt production rate as

was shown in Figure 7. The surface eruption rate is derived from the volcanic resurfacing rate (10^{-2} km²/yr, *Tanaka et al.* [1992]; *Hartmann and Neukum* [2001]) multiplied by the assumed thickness of the lava flows (3–10 m). The melt production rate in Figure 7 was derived from that assuming an eruption efficiency of 5–20% [*Kieffer*, 2003].

[46] We should reiterate that, at such low melt production rates, the allowable enrichment levels are strongly sensitive on the presumed solidus. For low solidus temperatures ($\sim 1100^\circ\text{C}$, *Bertka and Holloway* [1994], for an undepleted Martian mantle), the melt production rates are an order of magnitude in excess of those estimated for Mars, for all values of crustal enrichment. On the other hand, an extremely depleted Martian solidus (1440°C, *Musselwhite et al.* [2006], for the Yamato 980459 shergottite) produces no mantle melt for all crustal enrichment values. Unfortunately, no experimental constraints are, to date, available on intermediate, depleted representative Martian mantle solidi. Additionally, it has been suggested that the Martian mantle is fairly heterogeneous (cw. *Herd* [2003]), raising the question of whether a “representative” Martian solidus is a meaningful concept. In the absence of tighter constraints, we can only conclude that probable values of crustal enrichment on Mars which are consistent with the present volcanic rate are between 25 and 50%.

3.5. Composite Model

[47] While the previous models are sensitive to some parameters, in particular solidus temperatures, it is possible to construct a composite model that satisfies, within their uncertainties, all the given thermal and geological constraints for Mars. We use an Arrhenius viscosity, varying over 5 orders of magnitude (average interior viscosity 10^{21} Pas).

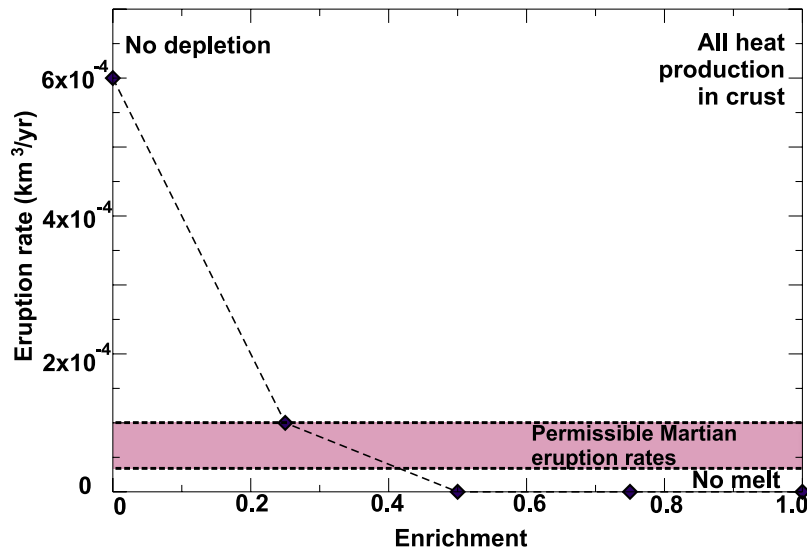


Figure 8. Surface eruption rate versus the level of crustal enrichment (0, no enrichment of HPEs into the crust; 1, all HPEs concentrated into the crust). For the model parameters listed in Table 1, with a surface solidus temperature of 1250°C. The range of permissible Martian eruption rates is calculated in the text. We find an enrichment value of 25–41% consistent with the recent volcanic record of Mars.

This gives as an average lithospheric thickness of ~200 km and a present-day heat flow of 25 mW/m², consistent with estimates from *McGovern et al.* [2002, 2004]. We assume the base of the Martian mantle is 1800°C, giving us a nonadiabatic temperature drop of 1547°C to drive convection. The average basal heat flow is less than 19 mW/m², which is sufficiently low that the outer core might not convect [*Nimmo and Stevenson, 2000*] and thus avoid generating a geody-

namo. We use an enrichment of 40% (i.e., 40% of HPEs are sequestered into the crust). Assuming a surface solidus temperature of 1200°C results in an eruption rate of 5×10^{-3} km³/yr, above our Amazonian estimates of $0.3\text{--}1 \times 10^{-4}$ km³/yr (section 3.3). However, adopting a surface solidus temperature of 1250°C results in an average eruption rate of 1×10^{-4} km³/yr, consistent with recent estimates.

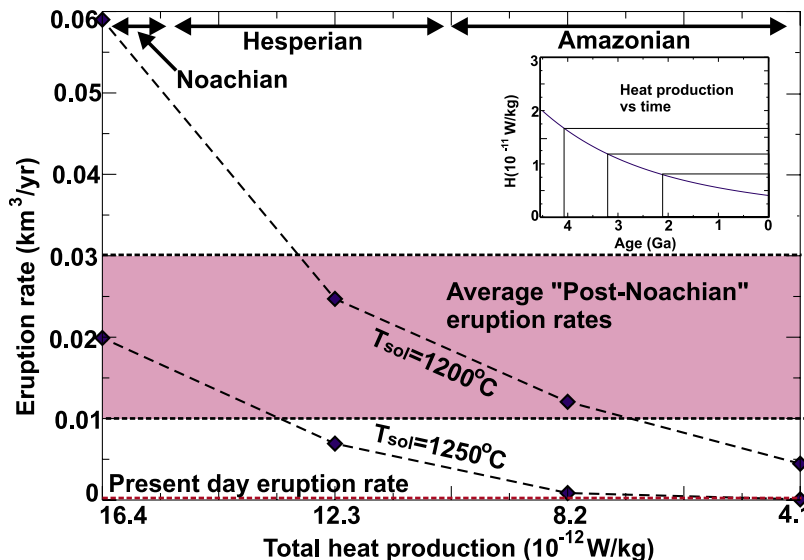


Figure 9. (a) Variation in total heat production versus time for the radioactivity model of *Wanke and Dreibus* [1994]. (b) Variation in surface eruption rate versus total mantle heat production for two different surface solidus temperatures (labeled) and an enrichment value of 40%. The 1200°C solidus fits the average “post-Noachian” global eruption rate of *Greeley and Schneid* [1991]. However, it overestimates the current (Amazonian) eruption rate (see text). A 1250°C solidus matches the present eruption rate well, though the average post-Noachian rate is below the Greeley and Schneid estimate. Given that the Martian solidus may be quite heterogenous, these models reproduce the decline in eruption rate through time extremely well.

[48] *Greeley and Schneider's* [1991] measured volume of post-Noachian volcanism is equivalent to an average extrusion rate of about $0.02 \text{ km}^3/\text{yr}$. For a plausible range of the ratio of intrusive to extrusive volcanism (5:1 to 12:1), this translates into an average total melt production volume of 0.11 to $0.24 \text{ km}^3/\text{yr}$, with a best estimate value of $0.17 \text{ km}^3/\text{yr}$. This is considerably more than the assumed recent eruption rate estimate, $\sim 1 \times 10^{-4} \text{ km}^3/\text{yr}$ [*Kiefer, 2003*] and suggests a considerable decline in volcanism over the last $\sim 3.5 \text{ Ga}$. We have used our "best fit" model parameters to calculate the average eruption rate through time in Figure 9. Here we increase the total heat production in the system back through time (Figure 9a), assuming a constant enrichment value. For a 1250°C surface solidus temperature, we fit the present-day eruption rates and satisfy the "post-Noachian" eruption rate estimates for the earliest Hesperian; however, the average integrated eruption rate is lower than *Greeley and Schneider's* estimate. For a 1200°C solidus, the average eruption rates are similar to *Greeley and Schneider's* estimate for much of the Amazonian and Hesperian, but this solidus overestimates the present-day eruption rates and the early Hesperian eruption rates, and the integrated eruption rate is higher than that of *Greeley and Schneider*. However, given the difficulties in constraining a representative Martian solidus and the uncertainties in eruption rate estimates, this example shows extremely well how the eruption rates on post-Noachian Mars may have varied for sensible model parameters.

4. Discussion

[49] By far the most sensitive influence on Martian melt production is the representative Martian solidus. In these models, the difference between calculated solidi for Mars (*Bertka and Holloway* [1994] versus *Musselwhite et al.* [2006]) results in either excessive amounts of melt or no melt at all. The variable degree of depletion observed in the Martian shergottites [*Musselwhite et al., 2006*] suggests that further models which include the ongoing depletion of the Martian mantle could shed light on heterogeneity in Martian melting conditions. Another critical aspect is the depth of the lithosphere, which constrains the depth to which warm mantle can ascend and thus melt production rates. Here this is determined self-consistently using temperature-dependent viscosity laws, but the choice of viscosity law markedly affects the lithospheric thickness. Our choice of an Arrhenius viscosity law, varying over 5 orders of magnitude for the temperature range considered, gives lithospheric thicknesses and surface heat flux values similar to estimates for Mars [*McGovern et al., 2002, 2004*].

[50] Within these bounds, we can also constrain the CMB temperatures, if we assume that 19 mW/m^2 is an upper bound, to be less than 1850°C . The basal heat flux is quite sensitive to this temperature. Furthermore, we estimate the enrichment of the Martian crust to be within the range 25–50%. Naturally this is contingent on the representative solidus and, to a lesser degree, lithospheric thickness. One aspect of this problem is to what extent does our Cartesian modeling domain affect the global energy budget? The problem is that for a Cartesian grid, the surface area at the top and bottom of the modeling domain are equal, while for a spherical planet with a core approximately one half of the planetary radius, the surface area at the bottom is a quarter

that of the top. If the system is purely basally heated, then the basal heat flux needs to be 4 times the surface heat flux at equilibrium, whereas for a Cartesian model they are equal.

[51] Of course, the Martian mantle is not solely basally heated but predominantly internally heated and with temperature-dependent viscosities. Such a system is subtly different, in that internal temperatures are largely governed by the rate of internal heating. The reason for this regulation was first espoused by *Tozer* [1972]: if the mantle is too hot, it will convect fast and lose its heat, lowering the internal temperatures. If it is too cold and not convecting fast enough, it will heat up, thus raising the internal temperatures. Thus the internal temperatures are strongly regulated by the internal heating rate. The internal heating rate is generally presented as a volumetric heating rate; and thus the geometry is somewhat peripheral to the determination of internal temperatures, which will, to first order, be dependent on volumetric heating rates and the temperature-dependence of viscosity. Naturally, additional basal heating will contribute to internal mantle temperatures, but most estimates for Earth at least suggest that this is a second-order contribution [*Sleep, 1992*].

[52] So to a first order, the mantle surface heat flux depends on the difference between mantle and surface temperatures and will be primarily determined on the internal temperatures, which are geometrically insensitive. Naturally the CMB heat flux has a contribution, but again sensible estimates suggest it is secondary [*Sleep, 1992*]. The CMB heat flux itself is determined by the temperature difference between the mantle and the core. That is, CMB heat flux should be primarily determined by a parameter that is geometrically insensitive. Furthermore, increased CMB heat flux would heat up the mantle, decreasing the temperature difference across the CMB, lowering the CMB heat flux. Thus there is a negative feedback in CMB heat flux, and it is strongly contingent on internal mantle temperatures, which should be largely geometrically insensitive. This broad argument is supported by the numerics. *Kiefer* [2003] has previously addressed similar problems in isoviscous systems in a two-dimensional hemispheric geometry, which is identical to a full spherical geometry for the purposes of heat flux. To give an example, model 4 in this paper gives a surface heat flux of 21.8 mW/m^3 and a basal heat flux of 33.3 mW/m^3 . The basal heat flux is only 1.5 times the surface heat flux rather than 4 times as per a purely bottom-heated system, supporting the contention that internal heating has a dominant role in determining CMB heat flux. This contrast drops even more for the higher internal temperatures of systems employing temperature-dependent viscosities.

[53] Another, related point is the extent to which melt production in our restricted, 4×1 boxes can be considered representative of Martian global averages. In all these simulations, melt production is restricted to a small number (1–3) of vigorous upwellings. A similar situation exists on Mars, where active volcanism is restricted to very few volcanic centers, and the bulk of recent Martian volcanism is concentrated around Tharsis [*Greeley and Schneider, 1991*]. We argue that the few active volcanic centers in our simulations are the equivalent, for purposes of eruption rate, of the volcanic centers on Mars. Obviously this is not

entirely satisfactory, and future work ideally would revisit this problem in a full three-dimensional spherical model.

[54] Our simplified dike propagation model excludes a number of effects that may be important for the localization and magnitude of surface eruptions. First, we assume vertical propagation only here. The reason for this is primary driving force for mantle dikes is the positive buoyancy of the melt. However, the ascent of dikes is strongly influenced by the ambient local stress field [Ito and Martel, 2002], and this is an effect that should be included in future models. Additionally, the propensity of dikes to take advantage of zones of lithospheric weakness (for example, preexisting fractures, etc.) is important for the surface distribution of volcanics and is another effect to consider in future work. None of these effects greatly affect our volcanic eruption rate estimates, however.

[55] A more significant effect is the response of propagating dikes to changes in density of the host rock. Here we are primarily concerned with the development and application of a model for the propagation of magma by interacting dikes from the mantle source region. We have neglected some details of the near-surface emplacement and assumed that the hot melt is at all times more buoyant than the host rock, an assumption that may not be valid for dikes propagating into low-density, differentiated crust. In this case, dikes may intrude at depth and never erupt on the surface. Future models would ideally recalculate the relative density of the dike and host rock as it ascended the rock column. Examples of dike emplacement models for Mars, including the effect of a neutral-buoyancy level, are given in the studies of Scott *et al.* [2002] and Wilson and Head [2002]. In terms of this work, the results may overestimate the volcanic eruption rate (for a given mantle melt production rate), though in a systematic way.

5. Martian Atmospheric Evolution

[56] The increased volcanic flux in the past obviously had an impact on the Martian atmosphere. However, the relationship between the rate of volcanism and the atmospheric pressure is complicated, and we will make a number of assumptions to simplify matters. Useful reviews of Martian atmospheric processes are in the studies of Jakosky and Phillips [2001] and Manning *et al.* [2006].

[57] To calculate Martian atmospheric pressures, we first consider a pure CO₂ atmosphere. While this may seem overly restrictive, CO₂ is the major atmospheric constituent today and was likely in the past also [Manning *et al.*, 2006]. Additionally, the complexities in the mechanisms of H₂O loss and the relative importance of other constituents are poorly constrained.

[58] We calculate the atmospheric pressure due to CO₂ as follows: we convert our rate of volcanism (in km³/yr) to kg/yr assuming a basaltic composition of extrusives. We then derive the mass of CO₂ generated for this volcanic mass, using CO₂ concentration estimates for volcanism on Earth (namely Iceland, $m_{\text{CO}_2} \sim 516$ mg/kg [Gslason *et al.*, 2002]). This, again, is a big assumption; there is no reason to believe that the CO₂ concentrations in Martian volcanoes are similar to Earth; however, in the absence of solubility models or specific constraints for Mars, this is a sensible estimate. This

then allows us to derive the volcanogenic contribution of CO₂ throughout the post-Noachian.

[59] We assume that the atmospheric pressure is directly related to the mass of CO₂ in the atmosphere, in the manner of Manning *et al.* [2006]:

$$P_{\text{CO}_2} = c m_g \quad (8)$$

[60] Presently, the atmosphere is at 6.8 mbar. Manning *et al.* [2006] estimate the present atmospheric mass (m_g) at 2.8×10^{16} kg, giving a constant c of 2.517×10^{-19} .

[61] To calculate the past atmospheric pressures, we must infer the loss rates of CO₂ from the atmosphere. A comprehensive summary of Martian CO₂ sinks is given by Manning *et al.* [2006]; we summarily bunch all the separate CO₂ sinks into one empirical loss term. Clearly, if the atmospheric pressure was greater in the past, then the CO₂ sinks must have overwhelmed the volcanogenic sources through time to result in a net atmospheric loss. Figure 10 shows the effect of different CO₂ sinks. The first example shows the effect of a constant CO₂ loss mechanism, with a magnitude equal to that of the greatest volcanogenic input rate. The maximum pressures reached (~ 70 mbar) fall well clear of one bar. In order for post-Noachian atmospheric pressures to ever exceed one bar, we need a recycling mechanism “15 times” the maximum volcanogenic input rate (series 2, Figure 10). With this constant loss rate of 1.32×10^{17} kg/yr, an atmospheric pressure of one bar is achievable just before 3 Ga.

[62] A constant loss rate is, however, extremely unrealistic, and so we have also included an example where the rate of CO₂ loss is a function of the atmospheric mass. Here

$$dm_g/dt = -0.15m_g \quad (9)$$

[63] In this case the constant is chosen to produce a similar final pressure (>1 bar) to the above example. However, the time at which the atmosphere reaches these pressures is significantly earlier (3.9 Ga), emphasizing the impact variable loss rates have on the magnitude and evolution of atmospheric pressures.

[64] Given the large uncertainties in CO₂ loss, we have not included the even more complex nature of a CO₂-H₂O atmosphere. While water is certainly lost more easily than CO₂, it is interesting to note that in most terrestrial volcanoes the concentration of water exceeds that of CO₂ by an order of magnitude [Stevenson and Blake, 1998]. While this might not be of relevance to a dry Mars today, in an early, degassing Martian mantle, this raises the possibility of a H₂O-driven greenhouse driven by massive volcanic outgassing (such as during Tharsis formation, Jakosky and Phillips [2001]). An interesting point to note is that the triple point for water (0.0098°C, 0.006 bar p_{H₂O}) does not actually require a significantly denser atmosphere, just warmer surface temperatures (cw. the CO₂ triple point at -56.4°C and 5.11 bar, Hoffman [2000]). In terms of atmospheric models, though, the most common way to achieve warmer temperatures is through a denser atmosphere [Jakosky and Phillips, 2001], though other alternatives include higher concentrations of potent greenhouse gases. Our simplistic treatment does not treat minor constituents such as methane,

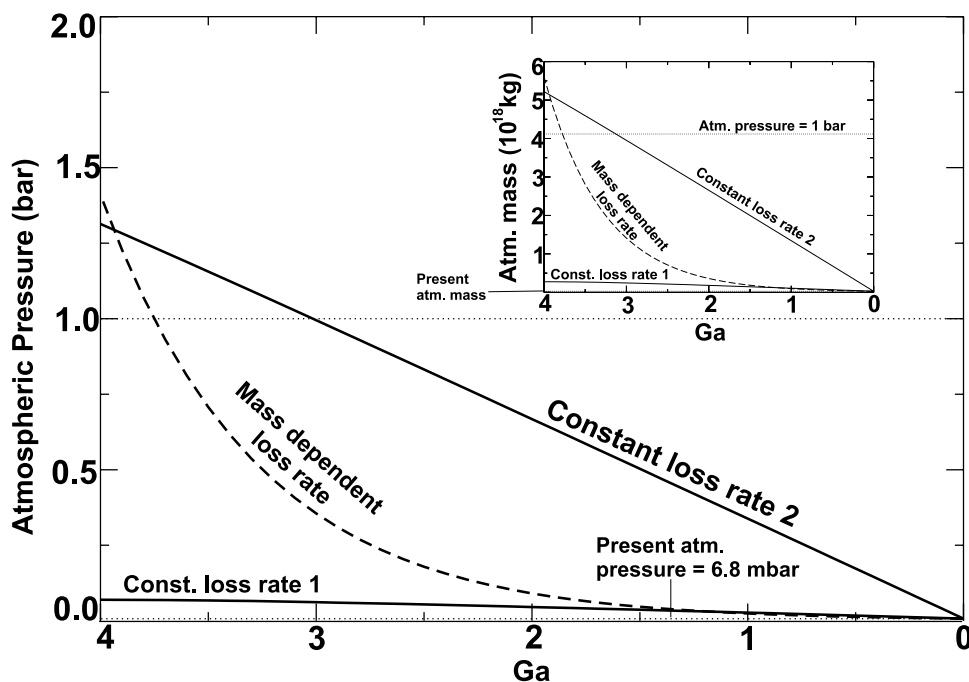


Figure 10. Post-Noachian atmospheric evolution of Mars, based on the rates of volcanism of Figure 9. (a) Decline of atmospheric mass versus time, assuming a dominantly CO_2 atmosphere and a current atmospheric mass of 2.8×10^{16} kg. The change in atmospheric mass is a combination of volcanic outgassing and a generic “loss” mechanism. The first loss mechanism (1) assumes that the loss rate is constant and equal to the maximum volcanic outgassing rate. The second (2) assumes that the loss rate (1.32×10^{17} kg/yr) is 15 times the maximum volcanogenic input. The third loss mechanism assumes that the rate of loss is proportional to the mass of the atmosphere [equation (9)]. (b) Atmospheric pressure versus time for the three examples shown in Figure 10a. In order for atmospheric pressures to exceed 1 bar in the early Hesperian, the average atmospheric loss rate since then must have exceeded the maximum volcanogenic input rate by 15 times.

sulfur dioxide (or sulfides), or indeed the effects of clouds [Forget and Pierrehumbert, 1997]. Our volcanic outgassing predictions do, however, provide a more realistic input for more advanced, future atmospheric evolution calculations.

6. Conclusions

[65] We have used available thermal and geologic constraints to constrain mantle convection models of Mars’ post-Noachian stagnant-lid evolution. We calculate the melt production rates for Mars’ thermal state now and in the past and use a dike-propagation algorithm to convert mantle melt production rates into volcanism rates. We find a parameter range which satisfies all of Mars’ thermal, geophysical, and petrological constraints and extend our models into the past by increasing mantle heat production to model Martian volcanism through time.

[66] We have found that lithospheric thicknesses ~ 200 km (heat flux 25 ± 5 mW/m²) satisfy present-day rates of volcanism; however, the degree of volcanism is strongly sensitive on the solidus temperatures. Additionally, temperatures at the CMB must presently be less than $\sim 1850^\circ\text{C}$ to satisfy geodynamo constraints. Crustal enrichment on Mars must be between 25 and 50% in order to satisfy melt production rates for sensible lithospheric thicknesses and solidus temperatures. Extended to past conditions, our models show a decline in volcanism rate from >0.17 km³/yr,

for the Hesperian, to $\sim 1 \times 10^{-4}$ km³/yr at present. The CO_2 flux would have declined from 8.83×10^7 kg/yr to 6.67×10^6 kg/yr during the same interval. In order to satisfy the constraints of (1) a present atmospheric pressure of 6.8 mbar and (2) an atmospheric pressure of over one bar at the start of the Hesperian, the average CO_2 loss rate (including all CO_2 sinks) must have been 15 times the maximum volcanogenic input rate. Volcanism, degassing, and crustal production are all important processes related to a planetary mantle’s evolution, and our dike-propagation model provides a self-consistent technique to relate these processes to long-timescale mantle convection.

[67] **Acknowledgments.** C.O’N. & A.L. acknowledge the support of NASA-MDAP grant NAG5-12166 & NSF Grant EAR-0448871. A.M.J. acknowledges the assistance of the NSERC and The Canadian Institute for Advanced Research. W.S.K. is supported by NASA Mars Fundamental Research Program grant NNG05GM15G. This is GEMOC ARC National Key Centre publication 463.

References

- Agee, C. B., and D. S. Draper (2004), Experimental constraints on the origin of Martian meteorites and the composition of the Martian mantle, *Earth Planet. Sci. Lett.*, *224*, 415–429.
- Bertka, C. M., and J. R. Holloway (1994), Anhydrous partial melting of an iron-rich mantle I: Subsolidus phase assemblages and partial melting phase relationships at 10 to 30 kbar, *Contrib. Mineral. Petrol.*, *115*, 313–322.
- Borg, L. E., J. E. Edmunson, and Y. Asmeron (2005), Constraints on the U-Pb isotopic systematics of Mars inferred from a combined U-Pb, Rb-Sr

- isotopic study of the Martian meteorite Zagami, *Geochim. Cosmochim. Acta*, **69**, 5819–5830.
- Bourdon, B., S. P. Turner, and N. M. Ribe (2005), Partial melting and upwelling rates beneath the Azores from a U-series isotope perspective, *Earth Planet. Sci. Lett.*, **239**, 42–56.
- Carr, M. H. (1996), *Water on Mars*, 229 pp., Oxford Univ. Press, New York.
- Carr, M. H., and H. Wanke (1992), Earth and mars: Water inventories as clues to accretional histories, *Icarus*, **98**, 61–71.
- Catling, D. C. (2004), On Earth, as it is on Mars?, *Nature*, **249**, 707–708.
- Ernst, R. E., E. B. Grosfils, and D. Mege (2001), Giant dike swarms: Earth, Venus, and Mars, *Annu. Rev. Earth Planet. Sci.*, **49**, 489–534.
- Forget, F., and R. T. Pierrehumbert (1997), Waring early Mars with carbon dioxide clouds that scatter radiation, *Science*, **278**, 1273–1276.
- Formisano, V., S. Atreya, T. Encenaz, N. Ignatiev, and M. Giuranna (2004), Detection of methane on Mars, *Science*, **306**, 1758–1761.
- Garvin, J. B., S. E. H. Sakimoto, J. J. Frawley, C. C. Schnetzler, and H. M. Wright (2000), Topographic evidence for geologically recent near-polar volcanism on Mars, *Icarus*, **145**, 648–652.
- Greeley, R., and B. D. Schneid (1991), Magma generation on Mars: Amounts, rates, and comparisons with Earth, Moon, and Venus, *Science*, **254**, 996–998.
- Gslason, S. R., A. Snorrason, H. K. Kristmannsdottir, A. E. Sveinbjornsdottir, P. Torsander, J. Olafsson, S. Castet, and B. Dupre (2002), Effects of volcanic eruptions on the CO₂ content of the atmosphere and the oceans: The 1996 eruption and flood within the Vatnajokull Glacier, Iceland, *Chem. Geol.*, **190**, 181–205.
- Hartmann, W. K., and G. Neukum (2001), Cratering chronology and the evolution of Mars, *Space Sci. Rev.*, **96**, 165–194.
- Heironymus, C. F., and D. Bercovici (1999), Discrete alternating hotspot islands formed by interaction of magma transport and lithospheric flexure, *Nature*, **397**, 604–607.
- Hieronymus, C. F., and D. Bercovici (2001), A theoretical model of hotspot volcanism: Control on volcanic spacing and patterns via magma dynamics and lithospheric stresses, *J. Geophys. Res.*, **106**(B1), 683–702.
- Herd, C. D. K. (2003), The oxygen fugacity of Olivine-Phyric Martian basalts and the components within the mantle and crust of Mars, *Meteorit. Planet. Sci.*, **38**, 1793–1805.
- Hirschmann, M. (1995), Melt pathways in the mantle, *Nature*, **375**, 737–738.
- Hoffman, N. (2000), White Mars: A new model for Mars' surface and atmosphere based on CO₂, *Icarus*, **146**, 326–342.
- Ito, G., and S. J. Martel (2002), Focusing of magma in the upper mantle through dike interaction, *J. Geophys. Res.*, **107**(B10), 2223, doi:10.1029/2001JB000251.
- Jakosky, B. M., and R. J. Phillips (2001), Mars' volatile and climate history, *Nature*, **412**, 237–244.
- Jaques, A. L., and D. H. Green (1980), Anhydrous melting of peridotite at 0–15 Kbar pressure and the genesis of tholeiitic basalts, *Contrib. Mineral. Petrol.*, **73**, 287–310.
- Jellinek, A. M., and D. J. DePaolo (2003), A mode for the origin of large silicic magma chambers: precursors of caldera-forming eruptions, *Bull. Volcanol.*, **65**, 363–381.
- Karato, S. I., and P. Wu (1993), Rheology of the upper mantle—A synthesis, *Science*, **260**, 771–778.
- King, S. D., and G. Masters (1992), An inversion for radial viscosity structure using seismic tomography, *Geophys. Res. Lett.*, **19**, 1551–1554.
- Kelemen, P. B., N. Shimizu, and V. J. M. Salters (1995), Extraction of mid-ocean-ridge basalt from the upwelling mantle by focused flow of melt in dunite channels, *Nature*, **375**, 747–753.
- Kiefer, W. S. (2003), Melting in the Martian mantle: Shergottite formation and implications for present-day mantle convection on Mars, *Meteorit. Planet. Sci.*, **38**, 1815–1832.
- Lister, J. R. (1990), Buoyancy-driven fluid fracture: Similarity solutions for the horizontal and vertical propagation of fluid-filled cracks, *J. Fluid Mech.*, **217**, 213–239.
- Lister, J. R. (1994), The solidification of buoyancy-driven flow in a flexible-walled channel, Part 1. Constant-volume, *J. Fluid Mech.*, **272**, 21–44.
- Lodders, K., and B. Fegley (1997), An oxygen isotope model for the composition of Mars, *Icarus*, **126**, 373–394.
- Lunine, J. I., J. Chambers, A. Morbidelli, and L. A. Leshin (2003), The origin of water on Mars, *Icarus*, **165**, 1–8.
- Lyons, J. R., C. Manning, and F. Nimmo (2005), Formation of methane on Mars by fluid-rock interaction in the crust, *Geophys. Res. Lett.*, **32**, L13201, doi:10.1029/2004GL022161.
- Manning, C. V., C. P. McKay, and K. J. Zahnle (2006), Thick and thin models of the evolution of carbon dioxide on Mars, *Icarus*, **180**, 38–59.
- Marti, K., and K. J. Mathew (2000), Ancient Martian nitrogen, *Geophys. Res. Lett.*, **27**, 1463–1466.
- Mathew, K. J., and K. Marti (2001), Early evolution of Martian volatiles: Nitrogen and noble gas components in ALH84001 and Chassigny, *J. Geophys. Res.*, **106**, 1401–1422.
- McGovern, P. J., et al. (2002), Localized gravity/topography admittance and correlation spectra on Mars: Implications for regional and global evolution, *J. Geophys. Res.*, **107**(E12), 5136, doi:10.1029/2002JE001854.
- McGovern, P. J., et al. (2004), Correction to “Localized gravity/topography admittance and correlation spectra on Mars: Implications for regional and global evolution”, *J. Geophys. Res.*, **109**, E07007, doi:10.1029/2004JE002286.
- McKenzie, D., and M. J. Bickle (1988), The volume and composition of melt generated by extension of the lithosphere, *J. Petrol.*, **29**, 625–679.
- McLennan, S. M. (2001), Crustal heat production and the thermal evolution of Mars, *Geophys. Res. Lett.*, **28**, 4019–4022.
- Moresi, L.-N., and V. S. Solomatov (1995), Numerical investigation of 2D convection with extremely large viscosity variations, *Phys. Fluids*, **7**, 2154–2162.
- Moresi, L., F. Dufour, and H.-B. Muhlhaupt (2003), A Lagrangian integration point finite element method for large deformation modeling of viscoelastic geomaterials, *J. Comput. Phys.*, **184**, 476–497.
- Musselwhite, Donald S., Heather A. Dalton, Walter S. Kiefer, and Allan H. Treiman (2006), Experimental petrology of the basaltic Shergottite Yamato 980459: Implications for the thermal structure of the Martian mantle, *Meteorit. Planet. Sci.*, **41**, 1271–1290.
- Neukum, G., et al. (2004), Recent and episodic volcanic and glacial activity on Mars revealed by the high resolution stereo camera, *Nature*, **432**, 971–979.
- Neumann, G. A., M. T. Zuber, M. A. Wieczorek, P. J. McGovern, F. G. Lemoine, and D. E. Smith (2004), Crustal structure of Mars from gravity and topography, *J. Geophys. Res.*, **109**(E8), E08002, doi:10.1029/2004JE002262.
- Nimmo, F., and D. J. Stevenson (2000), Influence of early plate tectonics on the thermal evolution and magnetic field of Mars, *J. Geophys. Res.*, **105**, 11,969–11,979.
- Norman, M. D. (1999), The composition and thickness of the crust of Mars estimated from rare Earth elements and neodymium isotopic compositions of Martian meteorites, *Meteorit. Planet. Sci.*, **34**, 439–449.
- O'Neill, C. J., L. Moresi, and A. L. Jaques (2005), Geodynamic controls on diamond deposits: Implications for Australian occurrences, *Tectonophysics*, **404**, 217–236.
- Reese, C. C., V. S. Solomatov, and L. Moresi (1999), Non-Newtonian stagnant lid convection and magmatic resurfacing on Venus, *Icarus*, **139**, 67–80.
- Rubin, A. M. (1995), Propagation of magma-filled cracks, *Annu. Rev. Earth Planet. Sci.*, **23**, 287–336.
- Rubin, A. M. (1998), Dike ascent in partially molten rock, *J. Geophys. Res.*, **103**(B9), 20,901–20,919.
- Rubin, K. H., and J. D. MacDougall (1988), ²²⁶Ra excesses in mid-ocean-ridge basalts and mantle melting, *Nature*, **335**, 158–161.
- Sato, K., and T. Hashida (2006), Cohesive crack analysis of toughness increase due to confining pressure, *Pure Appl. Geophys.*, doi:10.1007/s00024-006-0060-2.
- Scott, E. D., L. Wilson, and J. W. Head III (2002), Emplacement of giant radial dikes in the northern Tharsis region of Mars, *J. Geophys. Res.*, **107**(E4), 5019, doi:10.1029/2000JE001431.
- Sleep, N. H. (1992), Hotspot volcanism and mantle plumes, *Annu. Rev. Earth Planet. Sci.*, **20**(19), 19–43.
- Sobolev, A. V., and M. Chaussidon (1996), H₂O concentrations in primary melts from supra-subduction zones and mid-ocean ridges: Implications for H₂O storage and recycling in the mantle, *Earth Planet. Sci. Lett.*, **137**, 45–55.
- Spohn, T. (1991), Mantle differentiation and thermal evolution of Mars, Mercury, and Venus, *Icarus*, **90**, 222–236.
- Squyres, S. W., et al. (2004), In situ evidence for an ancient aqueous environment at Meridiani Planum, Mars, *Science*, **306**, 1709–1714.
- Stevenson, D. S., and S. Blake (1998), Modelling the dynamics and thermodynamics of volcanic degassing, *Bull. Volcanol.*, **60**, 307–317.
- Stolper, E., D. Walker, B. H. Hager, and J. F. Hays (1981), Melt segregation from partially molten source regions: The importance of melt density and source region size, *J. Geophys. Res.*, **86**, 6261–6271.
- Takada, A. (1989), Magma transport and reservoir formation by a system of propagating cracks, *Bull. Volcanol.*, **52**, 118–126.
- Tanaka, K. L., D. H. Scott, and R. Greeley (1992), Global stratigraphy, in *Mars*, edited by H. H. Kiefer, B. M. Jakosky, C. W. Snyder, and M. S. Matthews, 345–382, Univ. of Ariz. Press, Tucson.
- ten Brink, U. (1991), Volcano spacing and plate rigidity, *Geology*, **19**, 397–400.
- Tozer, D. C. (1972), The present thermal state of the terrestrial planets, *Phys. Earth Planet. Inter.*, **6**, 182–197.

- Turcotte, D. L., and G. Schubert (1982), *Geodynamics: Applications of Continuum Physics to Geological Problems*, 450 pp, John Wiley, Hoboken, N. J.
- Turner, S., P. Evans, and C. Hawkesworth (2001), Ultrafast source-to-surface movement of melt at island arcs from ^{226}Ra - ^{230}Th systematics, *Science*, 292(5520), 1363–1366.
- Wanke, H., and G. Dreibus (1994), Chemistry and accretion history of Mars, *Philos. Trans. R. Soc. London A*, 349, 285–293.
- Watts, A. B., and S. Zhong (2000), Observations of flexure and the rheology of oceanic lithosphere, *Geophys. J. Int.*, 142(3), 855–875.
- Weizmann, A., D. J. Stevenson, D. Prialnik, and M. Podolak (2001), Modeling the volcanism on Mars, *Icarus*, 150, 195–205.
- Wilson, L., and J. W. Head III (2002), Tharsis-radial graben systems as the surface manifestation of plume-related dike intrusion complexes: Models and implications, *J. Geophys. Res.*, 107(E8), 5057, doi:10.1029/2001JE001593.
- Yung, Y. L., et al. (1988), HDO in the Martian atmosphere: Implications for the abundance of crustal water, *Icarus*, 76, 146–159.
- Zuber, M. T., et al. (2000), Internal structure and early thermal evolution of Mars from Mars Global Surveyor topography and gravity, *Science*, 287, 1788–1793.
-
- A. M. Jellinek, Department of Earth and Ocean Science, University of British Columbia, Vancouver, BC, Canada.
- W. S. Kiefer, Lunar and Planetary Science Institute, Houston, TX, USA.
- A. Lenardic, Department of Earth Sciences, Rice University, Houston, TX 77005, USA.
- C. O'Neill, GEMOC ARC National Key Centre, Macquarie University, NSW, Australia. (conecill@els.mq.edu.au)